Heterogeneous Ice Nucleation Rate Coefficient of Water Droplets Coated by a Nonadecanol Monolayer

B. Zobrist,[†,‡] T. Koop,[‡] B. P. Luo,[†] C. Marcolli,[*,†] and T. Peter[†]

Institute for Atmospheric and Climate Science (IAC), ETH Zurich, Switzerland, and Department of Chemistry, Bielefeld University, Bielefeld, Germany

Received: September 18, 2006; In Final Form: November 8, 2006

The heterogeneous ice nucleation rate coefficient (j_{het}) of water droplets coated with a monolayer of 1-nonadecanol was determined from multiple freezing/melting cycles. Freezing was monitored optically with a microscope for droplet radii between 31 and 48 μm and with a differential scanning calorimeter for radii between 320 and 1100 μm. The combination of these two techniques allows the surface area of the 1-nonadecanol nucleating agent to be varied by more than a factor of 1000, showing that j_{het} increases only by ~5 orders of magnitude over a temperature range of 18 K. This is roughly 5 times less than the change in the ice nucleation rate coefficient for homogeneous ice freezing at around 238 K or for heterogeneous ice freezing in the presence of a solid ice nucleus, such as Al_2O_3. This temperature dependence of j_{het} can be reconciled with the framework of classical nucleation theory, when assuming a reduced compatibility of the alcohol monolayer with the ice embryo as the temperature decreases. We attribute this finding to an enhanced ability of the alcohol monolayer to adapt to the ice structure close to the ice melting point due to larger thermal density fluctuations in the monolayer, which in turn makes the monolayer serve as a better ice nucleus.

Introduction

Ambient temperatures on Earth drop regularly below the ice melting point. However, just as most other liquids, water and aqueous solutions do not readily freeze below the melting point, but rather can be supercooled to form metastable liquids.[1] Hence, it is important to understand the process of ice nucleation of water and aqueous solutions at subzero temperatures. Ice can form in the presence or absence of so-called ice nuclei (IN), leading to homogeneous or heterogeneous ice nucleation, respectively. IN are particles or structures (such as a monolayer) that accelerate the ice nucleation process by providing surfaces that facilitate the formation of the first ice germ. For example, natural IN are involved in the formation of glaciated clouds at temperatures above the homogeneous ice nucleation threshold (ca. −38 °C), thereby triggering the formation of precipitation and dehydration influencing the Earth's radiation budget.[2] In addition, IN also affect biological processes. Bacteria of the type *Pseudomonas syringae*, for example, use their ability to nucleate ice at small supercoolings to damage the tissues of fruits. These bacteria are now commercially employed as IN for artificial snow (Snomax, York International). Also, some high alpine plants in Africa have developed an elaborate strategy to overcome the diurnal cycle of the air temperature above and below 0 °C: Highly potent IN, most likely proteins, lead to ice freezing in the fluids inside the cylindric inflorescence as soon as the air temperature drops below 0 °C.[3] The latent heat release accompanying this freezing keeps the plant temperature at 0 °C even if the ambient air temperature falls to −10 °C. In this way, the plant avoids intracellular ice formation, which is often lethal to biological tissues.[4]

The complex structure as well as the chemical diversity of natural IN complicate theoretical descriptions of the ice nucleation process. One strategy is to employ model substances that mimic the properties of natural IN. One such a type of IN are self-assembling amphiphilic molecules at the surface of water droplets which induce ice nucleation at temperatures up to −1 °C in a very reproducible manner.[5] The structural match between the ice lattice and the 2D crystalline structure of a Langmuir film formed by long-chain alcohols has been identified as the key reason for the good ice nucleation ability of such monolayers.[6,7] However, there are other influencing factors that are less well understood, such as the effects of the length of the hydrocarbon chains, the orientation of the hydroxyl end groups with respect to each other and with respect to the air/water interface, and the molecular motion of the surfactant molecules at the air/water interface. Recently, the nucleation rates of single water droplets ($r \approx 1600$ μm) coated with various long-chain alcohols have been reported over a temperature range of 261−268 K.[8] In the present work, the previous studies are extended by varying the droplet size (31−1100 μm) and the investigated temperature range (248−266 K). We also show that the results obtained may be well described by classical nucleation theory.

Theoretical Considerations

In the framework of classical nucleation theory (CNT), the heterogeneous ice nucleation rate coefficient for supercooled water in contact with an ice nucleus, $j_{het}(T)$, can be described by[9]

$$j_{het}(T) = \frac{kT}{h} \exp\left[-\frac{\Delta F_{diff}(T)}{kT}\right] \times n \exp\left[-\frac{\Delta G(T)\, f_{het}}{kT}\right] \quad (1)$$

* Address correspondence to this author. E-mail: claudia.marcolli@env.ethz.ch.
† Institute for Atmospheric and Climate Science.
‡ Bielefeld University.

10.1021/jp066080w CCC: $37.00
Published on Web 01/11/2007

where k and h are the Boltzmann and the Planck constant, respectively, T is the absolute temperature, n ($\approx 10^{15}$ cm^{-2}) is the number density of water molecules at the ice nucleus/water interface, $\Delta F_{diff}(T)$ is the diffusion activation energy of a water molecule to cross the water/ice embryo interface, and $\Delta G(T)$ is the Gibbs free energy for the formation of the critical ice embryo in the absence of a heterogeneous ice nucleus. The compatibility function f_{het} (≤ 1) describes the reduction of the Gibbs energy barrier due to the presence of an ice nucleus. j_{het} is defined as the number of nucleation events per area of the ice nucleus and time (in our case cm^{-2} s^{-1}). The product of the rate coefficient with the area of the ice nucleus yields the number of frozen particles per unit time at a specific temperature. The first term in eq 1 characterizes the diffusive flux of water molecules to the ice embryo during its nascency, and the second describes the concentration of critical (viable) embryos at the nucleus/water interface. In the following, parametrizations for both exponential terms are developed.

The diffusion activation energy is defined as[10]

$$\Delta F_{diff}(T) = \frac{\partial \ln D(T)}{\partial T} kT^2 \tag{2}$$

where D is the diffusivity of water, which can be expressed by the empirical Vogel−Fulcher−Tammann equation as[11]

$$D(T) = D_0 \exp\left[-\frac{E}{T - T_0}\right] \tag{3}$$

where D_0, E, and T_0 are fit parameters. Thus, eq 2 can be rewritten as

$$\Delta F_{diff}(T) = \frac{kT^2 E}{(T - T_0)^2} \tag{4}$$

For liquid water, the values of $E = 892$ K and $T_0 = 118$ K have been determined experimentally by Smith and Kay[11] in the temperature range from 150 to 273 K.

In CNT, $\Delta G(T)$ is given by[12]

$$\Delta G(T) = \frac{16\pi}{3} \frac{v_{ice}^2(T)\sigma_{sl}^3(T)}{[kT \ln S(T)]^2} \tag{5}$$

where $v_{ice}(T)$ is the volume of a H_2O molecule in ice, $\sigma_{sl}(T)$ is the interfacial tension between water and the ice embryo, and $S(T)$ is the ice saturation ratio. Parametrizations for these variables as a function of temperature are given below.

The volume of a H_2O molecule in ice [cm^3] is parametrized by fitting data of the density of ice in the supercooled regime,[13] leading to

$$v_{ice}(T) = \frac{M_w}{N_a \rho_0}(1 - 0.05294T_r - 0.05637T_r^2 - 0.002913T_r^3)^{-1} \tag{6}$$

M_w is the molar mass of water, N_a is the Avogadro constant, ρ_0 is the density of ice at the ice melting point T_m^0, and the reduced temperature T_r is given by $T_r = (T - T_m^0)/T_m^0$.

The interfacial tension σ_{sl} is poorly quantified in the supercooled region for two reasons. First, the ice embryo can be as small as or even smaller than 1 nm in radius, so that σ_{sl} may differ from the macroscopic interface energy. Second, the macroscopic interface energy between water and bulk ice has only been measured at 273.15 K and not in the supercooled regime. Therefore, we derived this quantity by fitting measurements of the homogeneous ice nucleation rate coefficient of Pruppacher et al.,[9] Krämer et al.,[14] Duft and Leisner,[15] Benz et al.,[16] Stöckel et al.,[17] and Kabath et al.[18] using eq 1 with $f_{het} = 1$ and $n = 3.1 \times 10^{22}$ cm^{-3} (volume number density of water molecules in liquid water). This yields

$$\sigma_{sl}(T) = [3.298 \times 10^{-6} + (1.2048 \times 10^{-6})T_r - (4.6705 \times 10^{-5})T_r^2] \text{ J cm}^{-2} \tag{7}$$

applicable in the temperature range of 229 K $\leq T \leq$ 238 K. The extrapolation of this parametrization to the melting temperature T_m^0 yields a value of 3.298×10^{-6} J cm^{-2}. This is in very good agreement with the experimental measurement of σ_{sl} at T_m^0 by Hobbs et al.[19] ($(3.3 \pm 0.3) \times 10^{-6}$ J cm^{-2}), allowing us to apply the parametrization over the whole supercooled temperature range up to T_m^0.

The ice saturation ratio S in pure liquid water is defined as

$$S(T) = \frac{p_{H_2O}(T)}{p_{ice}(T)} \tag{8}$$

where p_{H_2O} and p_{ice} are the vapor pressures of supercooled liquid water and ice, respectively. We have used the most recent parametrizations for p_{H_2O} and p_{ice} given by Murphy and Koop:[20]

$$\ln[p_{ice}(T)] = 9.550426 - 5723.265/T + 3.53068 \ln(T) - 0.00728332T \tag{9}$$

and

$$\ln[p_{H_2O}(T)] \approx 54.842763 - 6763.22/T - 4.210 \ln(T) + 0.000367T + \tanh[0.0415(T - 218.8)](53.878 - 1331.22/T - 9.44523 \ln(T) + 0.014025T) \tag{10}$$

where T is in Kelvin and p in Pa.

Finally, the compatibility function f_{het} may be described as[12]

$$f_{het} = \frac{1}{4}(2 + \cos\alpha)(1 - \cos\alpha)^2 \tag{11}$$

The parameter α may be interpreted as a contact angle. For gas-to-liquid nucleation, α is given in terms of the interfacial tensions for the different phases (so-called "Young's relation") and can exhibit values between 0 and 180°, leading to values of 0 to 1 for f_{het}, respectively. In the case of liquid-to-solid nucleation, α formally represents the contact angle between the ice embryo and the ice nucleus in an aqueous medium, i.e., between a solid phase and the alcohol monolayer. This angle is not measurable in a macroscopic way. Therefore we term α as the effective contact angle, and use it as a convenient parametrization of the compatibility function, subsuming all specific ice nucleation effects of an individual ice nucleus. Thus, $\alpha = 0°$ implies perfect compatibility between the ice nucleus and the ice, and consequently a vanishing free energy for the formation of the critical ice embryo, and a nucleation process that is only limited by diffusion. Conversely, $\alpha = 180°$ means that the Gibbs formation energy is not reduced at all by the presence of the ice nucleus, equivalent to homogeneous ice nucleation.

Data Evaluation Procedure

Following Koop et al.,[21] the ice nucleation rate ω [s^{-1}] can be determined by using Poisson statistics from a series of single freezing point measurements:

$$\omega = \frac{n_{\mathrm{nuc}}}{t_{\mathrm{tot}}} \tag{12}$$

where n_{nuc} is the number of nucleation events within the total observation time t_{tot}. We consider a process in which a constant cooling rate is applied to samples. There is no principal difference in evaluating j_{het} from continuous cooling experiments and constant temperature experiments, because j_{het} does not depend on the cooling rate. It was shown in other experimental studies that homogeneous ice nucleation rate coefficients determined from continuous cooling experiments are the same as those from constant temperature single droplet experiments (see, e.g., Krämer et al.[14]).

Different numbers of freezing events may occur in equally sized temperature intervals ΔT. The total observation time in the ith temperature interval, t^i_{tot}, is given by the sum of the contributions from the droplets that remain liquid and the droplets that freeze:

$$t^i_{\mathrm{tot}} = \frac{\Delta T}{c_{\mathrm{r}}}(n^i_{\mathrm{tot}} - n^i_{\mathrm{nuc}}) + \sum_{j=1}^{n^i_{\mathrm{nuc}}} \Delta t_{\mathrm{nuc},j} \tag{13}$$

Here, c_{r} is the experimental cooling rate, n^i_{tot} is the number of liquid samples at the beginning of the ith temperature interval, and n^i_{nuc} is the number of frozen samples at the end of the temperature interval. $\Delta t_{\mathrm{nuc},j}$ is the time it took the jth sample to nucleate within the ith temperature interval, i.e.

$$\Delta t_{\mathrm{nuc},j} = \frac{1}{c_{\mathrm{r}}}(T^i_{\mathrm{st}} - T^i_{\mathrm{nuc},j}) \tag{14}$$

where T^i_{st} is the starting temperature of the ith interval, and $T^i_{\mathrm{nuc},j}$ is the freezing temperature of the jth sample in the ith temperature interval.

The average heterogeneous ice nucleation rate coefficient, j_{het}, at the mean temperature T^i of the temperature interval is given by

$$j_{\mathrm{het}}(T^i) = \frac{\omega_{\mathrm{het}}(T^i)}{A_{\mathrm{IN}}} = \frac{n^i_{\mathrm{nuc}}}{t^i_{\mathrm{tot}}}\frac{1}{A_{\mathrm{IN}}} \tag{15}$$

where A_{IN} is the total surface area of the ice nucleus. It is justified to exclude the possible contribution of homogeneous ice nucleation because of the good ice nucleation ability of the investigated ice nucleus.

Once the experimental data have been analyzed with eq 15, the obtained values for j_{het} can be used to evaluate the effective contact angle α, the only unknown parameter in eq 1.

Experimental Section

Heterogeneous ice freezing points of water droplets coated with a nonadecanol/mineral oil solution were determined with two types of instruments. Smaller droplets ($r = 31-48$ μm) were investigated with a cooling stage (Linkam LTS 120) attached to an optical microscope (Olympus BX40). In these experiments freezing was detected optically. The temperature of the cooling stage was calibrated by using the melting points of six organic solvents (dodecane: Aldrich ≥99%; tetradecane: Merck > 99%; pentadecane: Sigma ≥99%; heptadecane: Fluka ≥98%; octadecane: Fluka puriss; and diphenyl ether: Aldrich ≥99%) yielding an accuracy of the reported freezing points of ±0.7 K. The larger droplets ($r = 320-1100$ μm) were studied with a differential scanning calorimeter (DSC; TA Instruments Q10) in which nucleation is detected by the latent heat that is released during freezing. The temperature calibration of the DSC was performed with the melting point of ice and the ferroelectric phase transition of $(NH_4)_2SO_4$ (Sigma-Aldrich, 99.99%+) at 223.1 K yielding an accuracy of the reported freezing points of ±0.5 K.

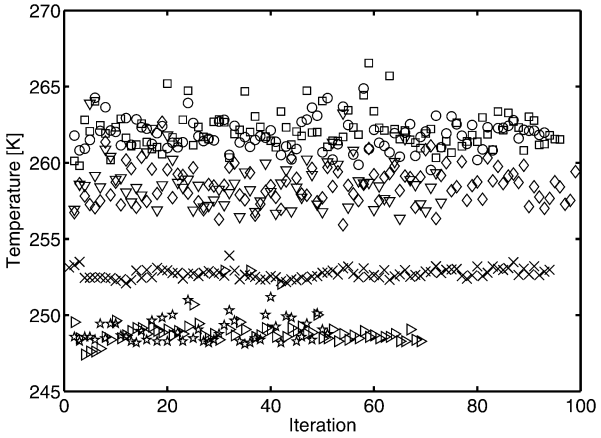

Figure 1. Measured freezing points for seven droplets exposed to cooling/heating cycles with 10 K min^{-1} as a function of iteration number. Six droplets are coated with 1-nonadecanol, one remained uncoated. Coated droplets: (circles and squares) $r = 1100$ μm; (diamonds and downward-pointed triangles) $r = 370$ and 320 μm, respectively; and (stars and right-pointed triangles) $r = 31$ and 48 μm, respectively. Uncoated droplet: (crosses) $r = 1100$ μm.

With use of a custom-made droplet generator,[22] the smaller droplets were deposited on a glassy microscope slide coated with a 150 nm aluminum and a 30 nm thick Al_2O_3 layer to increase the contrast for optical freezing detection. The larger droplets were produced directly into a standard aluminum DSC sample pan with use of a microliter pipet. All droplets were then immediately covered with ~50 μL of a 3.3×10^{-3} M solution of 1-nonadecanol (Fluka, purum) in mineral oil (Aldrich), resulting in a self-assembled nonadecanol monolayer at the interface between the water droplets and the mineral oil. The concentration of the nonadecanol/mineral oil solution was larger than required for a complete monolayer coverage of nonadecanol to ensure full coverage of the water droplets. The rest of the alcohol molecules were likely arranged as micelles in the oil. In all experiments a cooling rate of 10 K min^{-1} was used and after each freezing run, the sample was heated to 285 K with a heating rate of 10 K min^{-1}. The temperature at the onset of freezing was identified as the nucleation temperature.

Results

Heterogeneous freezing point measurements of water droplets covered with a nonadecanol/mineral oil solution are shown in Figure 1. Different symbols represent individual droplets with radii between 31 and 1100 μm that were frozen and melted repeatedly with total iteration numbers of up to 98 and a corresponding measurement time of up to 10 h.

The larger droplets show higher freezing temperatures than the smaller ones. Each time series in Figure 1 shows a scatter in freezing temperature as a function of iteration number, which can be attributed to the stochastic behavior of the nucleation

process (see below). The scatter becomes smaller with decreasing droplet radius and decreasing temperature. This might indicate a stronger temperature dependence of the nucleation rate coefficient at lower temperature. Also included in Figure 1 are the results from a droplet ($r = 1100$ μm) covered with pure mineral oil without nonadecanol. In this case heterogeneous ice nucleation occurs at the aluminum surface of the DSC pan (homogeneous ice nucleation would require $T \leq 240$ K). The freezing points of this droplet (crosses) are clearly below those of the nonadecanol coated droplets of the same size (circles or squares), showing that nonadecanol is a much better ice nucleus than the aluminum DSC pan and that the nucleation of droplets coated with nonadecanol is not affected by the presence of the aluminum surface. A similar test was performed for the small droplets deposited on a Al_2O_3 coated microscope slide. A droplet with a radius of $\sim$40 μm that was cycled a few times froze at temperatures $\sim$7 to 8 K lower than the droplets with nonadecanol coatings.

Experiments similar to those shown in Figure 1 have been reported by Gavish et al.[5] and by Seeley and Seidler.[8] However, in these studies only larger water droplets ($r \approx 1600$ μm) were investigated. In addition, the alcohol monolayer was arranged at the water/air interface and not at the water/mineral oil interface. In a previous study Popovitz-Biro et al.[23] reported a minor change in freezing temperature of water droplets with long-chain alcohols arranged at the interface between water and various liquids that are immiscible with water. The magnitude of this effect seemed to depend on the nature of the immiscible liquid. Experiments that we have performed with a nonadecanol monolayer arranged at the air/water interface of larger water droplets showed no significant difference in the freezing behavior from those with nonadecanol at the water/mineral oil interface on the basis of a Wilcoxon rank sum test on a 5% level.

However, water droplets with the monolayer arranged at an oil/water interface rather than at the air/water interface have two advantages. First, it is nearly impossible to cover droplets smaller than 100 μm with a nonadecanol monolayer at the air/water interface in a controlled and repeatable manner. Second, the effect of water evaporation during an experiment affects smaller droplets more strongly. Microscope photographs taken at the beginning and at the end of every series verified that the droplet size did not decrease due to water evaporation during the experiments. Moreover, linear fits through the individual data series did not show trends significantly different from zero (on the basis of a student's t-test on a 5% level), indicating no systematic change in the freezing temperature throughout an experiment.

In the analysis of the data shown in Figure 1, the first freezing point in each series was omitted. This was done because Seeley and Seidler[24] have reported that the freezing temperature of droplets coated with long-chain alcohols at the air/water interface depends on the highest temperature that the droplet experienced between two cooling cycles. This was attributed to a preactivation, once ice had formed for the first time beneath the monolayer. Our experiments support this observation, since the first freezing point in each series is distinctly lower than the rest of the series. Consequently these points are not shown in Figure 1 and are omitted for the following analysis procedure.

Because no systematic changes occurred from one freezing cycle to the next, we treat the freezing point measurements in Figure 1 as a series of independent and identically conditioned experiments and, therefore, analyze them using Poisson statistics. We have divided each series into 4−5 equally sized temperature intervals and evaluated the data according to eq 15, resulting in a mean rate coefficient for heterogeneous ice nucleation, j^i_{het}, in each interval i within a series (see Table 1). Each droplet is in contact with two interfaces, the substrate and the nonadecanol/oil. For the analysis we assume A_{IN} to be equal to the interface area between the droplet and the nonadecanol/oil layer for the coated droplets, and equal to the aluminum area covered by the droplet for the uncoated case. From the j^i_{het} values determined from the measurements we calculate the compatibility function for both types of ice nuclei, aluminum and nonadecanol, according to eqs 1 and 11.

TABLE 1: Analysis of Ice Nucleation Properties of Droplets Coated with Nonadecanol in Comparison with an Uncoated Water Droplet[a]

interval i	n^i_{nuc}	T^i [K]	log j^i_{het} [cm^{-2} s^{-1}]	α
uncoated droplet				
$r = 1100$ μm, $n_{tot} = 93$				
1	31	252.3	1.168	63.7
2	46	252.8	0.605	63.2
3	13	253.2	−0.138	62.9
4	3	253.7	−0.803	62.4
droplets coated with nonadecanol monolayer				
$r = 1100$ μm, $n_{tot} = 92$				
1	10	260.1	0.792	47.3
2	31	261.1	0.416	45.3
3	36	262.2	0.087	43.1
4	11	263.3	−0.571	41.0
5	4	264.4	−1.041	38.7
$r = 1100$ μm, $n_{tot} = 95$				
1	18	260.5	0.701	46.5
2	50	261.8	0.267	43.8
3	18	263.2	−0.436	41.1
4	7	264.5	−0.895	38.2
5	2	265.9	−1.460	35.1
$r = 370$ μm, $n_{tot} = 98$				
1	14	256.6	1.633	54.1
2	39	258.0	1.218	51.5
3	33	259.3	0.824	48.9
4	10	260.7	0.191	46.4
5	2	262.0	−0.528	43.9
$r = 320$ μm, $n_{tot} = 72$				
1	24	257.1	1.531	53.1
2	30	258.6	1.112	50.2
3	11	260.1	0.501	47.4
4	5	261.6	0.103	44.3
5	2	263.1	−0.312	41.2
$r = 48$ μm, $n_{tot} = 68$				
1	39	248.1	3.535	71.0
2	25	249.5	2.564	68.9
3	1	250.9	1.112	67.2
4	3	252.2	1.582	63.5
$r = 31$ μm, $n_{tot} = 50$				
1	30	248.5	3.787	69.8
2	11	249.3	3.060	68.8
3	7	250.0	2.748	67.4
4	2	250.8	2.170	66.2

[a] r: radius of the droplet. n_{tot}: total number of freezing events in a series. n^i_{nuc}: number of freezing events in a specific temperature interval. T^i: temperature at the center of an interval. j^i_{het}: calculated mean heterogeneous rate coefficient of a temperature interval at T^i. α: effective contact angle calculated with eqs 1 and 11.

Uncoated Droplet. For the droplet without nonadecanol coating, more than 80% of all freezing events occurred within a temperature interval of about 1 K indicating that the nucleation rate coefficient steeply increases with decreasing temperature, i.e., $\sim$2 orders of magnitude within a temperature interval of 1.4 K, see Table 1. This increase is comparable with that of the

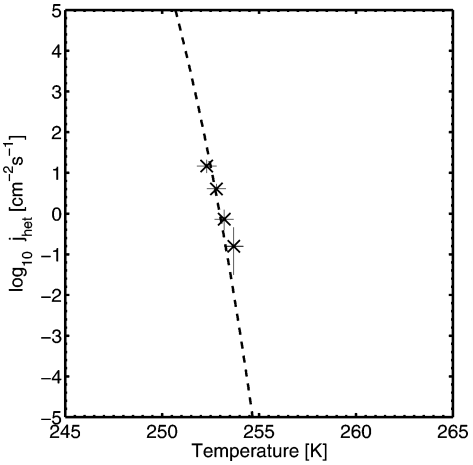

Figure 2. (Crosses) Measured heterogeneous ice nucleation rate coefficients for the droplet without nonadecanol as a function of temperature. (Dashed line) Calculated j_{het} with a constant α of 63.3°. The horizontal and vertical thin lines are the errors in the temperature measurements and the uncertainties due to Poisson statistics on the 95% level, respectively, showing larger uncertainties for the bins with a smaller number of freezing events.

homogeneous ice nucleation (∼2.1 orders of magnitude in 1.4 K in the temperature range between 233 and 243 K).[9] The curve shown in Figure 2 was calculated according to eq 1 with an effective contact angle of 63.3°, which was determined from the average of the four α-values in each of the four temperature intervals shown in Table 1 weighted by the number of freezing events per interval. Considering the experimental uncertainties, the measured j_{het} are well described by the calculated curve based on CNT with a constant effective contact angle.

Coated Droplets. As can be seen from Figure 3 and Table 1, the size and temperature dependence of j_{het} for droplets coated with nonadecanol differs distinctly from those without coating. Nucleation events for individual droplets are observed over a broader temperature range and j_{het} increases by only about 0.4 orders of magnitude within a temperature interval of 1.4 K when analyzed over the entire investigated temperature range.

Figure 3 shows the measured j_{het} in comparison with several calculations based on CNT with varying parametrizations for α. A constant α of 52.4° (obtained as an average by weighting the individual α values with the freezing events within a bin) results in a curve for j_{het} (dashed line) that cannot reproduce the measurements. The slope of the fit is much too steep. As mentioned before, the effective contact angle, if calculated separately for each temperature bin, strongly increases with decreasing temperature (see Table 1 and Figure 4). Therefore we included a linear temperature dependence of α. The resulting curve (solid line) describes the measurements far better. Most data points in Figure 3 are well reproduced by the solid curve, when we take uncertainties due to Poisson statistics on the 95% level and temperature uncertainties into account. This comparison shows that the temperature dependence of j_{het} is dominated by α, which becomes obvious by considering eq 1 in more detail: The term kTn/h depends only linearly on temperature and also $\Delta F_{diff}(T)$ increases only slightly with decreasing temperature ($\Delta F_{diff}(250K)/\Delta F_{diff}(265K) \simeq 1.1$). Thus, the term $\Delta G_{hom}\, f(\alpha)$ determines most of the temperature dependence of j_{het}, and a temperature dependence different from that of homogeneous ice nucleation can only be reached by introducing a temperature dependence for α.

An alternative approach was recently used by Seeley and Seidler.[8] They reported the temperature-dependent nucleation rates of single water droplets coated with a long-chain alcohol

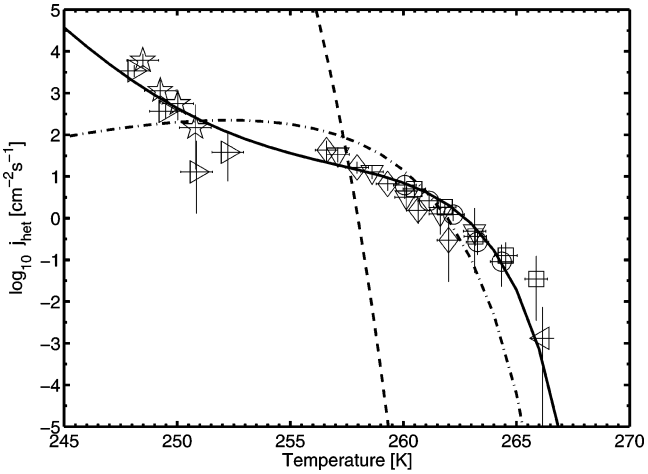

Figure 3. Measured heterogeneous ice nucleation rate coefficients for six single water droplets coated with nonadecanol as a function of temperature. The symbols are the same as in Figure 1. The horizontal and vertical thin lines are the errors in temperature and the uncertainties due to the Poisson statistics on the 95% level, respectively. Additionally, an isothermal measurement of j_{het} (left-pointed triangle) at 266.15 K is shown.[25] (Dashed line) Best fit of the CNT with a constant α of 52.4°. (Solid line) Best fit of the CNT with α as a linear function of temperature (see Figure 4). (Dashed dotted line) Best fit with the approach of Seeley and Seidler.[8]

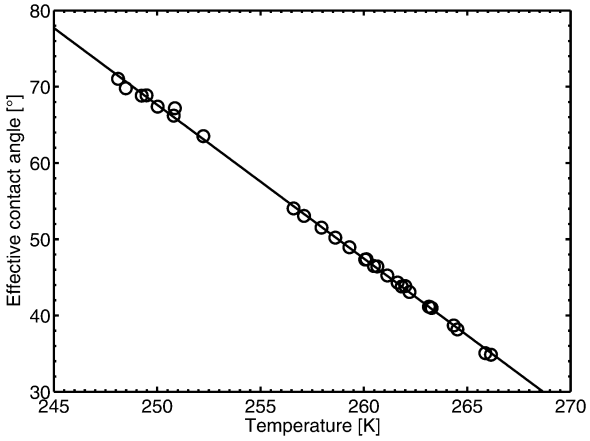

Figure 4. (Circles) Calculated α values for water droplets coated with nonadecanol as a function of temperature (see Table 1). (Solid line) Linear fit of the circles: $\alpha(T) = 571.50 - 2.015T$, where T is given in Kelvin. α is given in degree and the function is valid for 248 K ≤ T ≤ 268 K.

(C chain length varying from 25 to 28) over a temperature range from 261 to 268 K.[8] By reducing the prefactor ($kTn/h \exp[-\Delta F_{diff}(T)/kT]$) of eq 1 by 15 orders of magnitude, the authors were able to bring their measurements in accordance with CNT, while keeping α constant (with α values in a range between 19° and 31° for the different alcohols). This reduction was explained as a result of a hindered molecular diffusion of the water molecules to the interfacial plane, resulting from the dipole forces between the long-chain alcohol film and the interfacial water molecules. In Figure 3 this approach yields the dashed-dotted line, obtained by reducing the prefactor by 15 orders of magnitude and keeping α constant. At higher temperature, this results in a far better agreement with the measured j_{het} compared to the curve calculated without reduced prefactor (dashed line in Figure 3). However, the curve does not monotonously increase with decreasing temperature, which is clearly in contrast to our measurements, indicating that a reduction of the prefactor by a constant value cannot remove the discrepancy between CNT and the measurements.

We have re-evaluated the freezing point measurements of Seeley and Seidler[8] with a variable α, leading also to an increase in the effective contact angle with decreasing temperature for the C25−C28 alcohols. The temperature dependence of α for all alcohols is indeed similar to that of C19 investigated here, indicating a similar behavior for the five different alcohols. Note that the difference in α for different alcohols is distinctly smaller than the temperature dependence of α for an individual alcohol.

Discussion

So far, we have shown that the measured heterogeneous ice nucleation rate coefficient of differently sized droplets coated with various long-chain alcohols can be parametrized with a temperature-dependent α using CNT. But what causes this large increase of α with decreasing temperature?

The match between the ice lattice and the 2D crystalline structure of a Langmuir-like film formed by the long-chain alcohols has been identified as the key reason for the good ice nucleation ability of such monolayers.[5] The rectangular unit cell viewed along the *c*-axis exhibits values of $a = 4.86-5.05$ Å and $b = 7.45-8.41$ Å for long-chain alcohols with carbon chains from C16 to C31 at 278 K.[7] On the other hand, a *c*-centered rectangular cell in the hexagonal ice unit cell has $a_r = 4.52$ Å and $b_r = 7.83$ Å, suggesting a close structural match. The tilt angle of the alcohol molecules on the droplet surface, as well as the degree of order of the 2D lattice, the carbon chain length, and the different head group orientations resulting from odd or even C-numbers, have been identified as additional factors influencing the ice nucleation efficiency of long-chain alcohols.[5,6,7,26] Hence, no single structural attribute alone can explain the range of observed freezing temperatures within this class of compounds.[6] The alcohols with 30 and 31 C-atoms, for example, have almost identical lattice parameters and tilt angles,[7] but their heterogeneous freezing temperatures differ by about 7 K,[5] resulting from the different head group orientation.[6] This example indicates that small differences in the arrangement of the alcohols can result in a large difference in the heterogeneous freezing temperature. It has remained unresolved which structural parameter contributes most to the ice nucleation efficiency of long-chain alcohols and how these parameters may change with decreasing temperature.

There is evidence for a gradual change as a function of temperature in the structural arrangement of alcohol monolayers on water surfaces. Recently Ochshorn and Cantrell[27] demonstrated that infrared spectra of ~40-nm-water films covered by a layer of C17-alcohol show a continuous spectral shift from a band characteristic of liquid water to one characteristic of ice as the temperature is ramped from 263 to 256 K. The onset of this shift is at a temperature consistent with the freezing temperature reported by Popovitz-Biro et al.;[6] however, this might be accidental as the freezing temperature is strongly dependent on sample size as shown above. In addition to the changes in the water spectrum, analysis of the CH_2 stretching features in the alcohols' absorbance bands reveals simultaneous structural changes within the alcohol film. We note that in these experiments only 40-nm-thick water films were investigated, conditions which might hamper a direct comparability to our experiments. Nevertheless, these results point out the flexible structure and adaptability of such alcohol monolayers arranged at the water surface.

Seeley and Seidler[24] suggested a structural rearrangement within the alcohol monolayer as a cause for the preactivation, a phenomenon that was also observed in freezing point measurements for different long-chain alcohols in recent experiments by Cantrell and Robinson[28] and in our study. We propose that the interaction between the lattice of ice and the 2D crystalline monolayer allows for rearrangements leading to an enhanced ice nucleation efficiency of long-chain alcohols. While the formation of a critical embryo is favored by lower temperatures, the molecular rearrangement is favored by higher temperatures. Thus, the calculated α values in Table 1 may reflect the energy required for the rearrangement to induce a structural match, in accordance with the suggestion that α subsumes all ice nucleation effects of the nucleus. For an ice nucleus with a solid surface, e.g., Al_2O_3, no rearrangement can occur, which may be the reason why no temperature dependence of α was observed in this case.

According to CNT, the radius of the critical ice embryo, r_{crit}, decreases from 8.4 to 2.1 nm as the temperature is decreased from 266 to 248 K. This indicates that while j_{het} increases by 5 orders of magnitude, r_{crit} only decreases by a factor of 4. (Note that r_{crit} is identical for the cases of homogeneous and heterogeneous ice nucleation.) Therefore, we would expect that a smaller rearrangement is required to form a critical ice embryo at low temperature, thus leading to an improved ice nucleating ability. However, the opposite is observed, i.e., α increases with decreasing temperature. This observation implies that the flexibility of the alcohol monolayer to adapt to the ice structure is reduced at lower temperatures. While further structural investigations across a range of low temperatures will be required to understand the adaptive behavior of the ice/alcohol interface, the present study shows that monolayers of long-chain alcohols form a special set of ice nuclei, most likely due to their high flexibility and ability to adapt to the ice structure.

Conclusion

Heterogeneous ice freezing points of water droplets with radii $r = 31-1100$ μm coated with nonadecanol as heterogeneous ice nucleus have been analyzed with use of Poisson statistics. The experimentally determined heterogeneous ice nucleation rate coefficient shows a much weaker temperature dependence than homogeneous ice nucleation and heterogeneous freezing in the presence of a solid ice nucleus such as Al_2O_3. This behavior can be parametrized by using CNT assuming a linear dependence of the effective contact angle on temperature. A pronounced smooth change in the effective contact angle as a function of temperature has so far not been observed for other IN. The mobility of the long-chain alcohol molecules on the water surface may allow a rearrangement of the alcohol molecules at the water surface, resulting in a better match with the ice lattice and thus a higher freezing temperature. The increase of the effective contact angle with decreasing temperature is probably due to the decreasing mobility of the alcohol molecules. Theoretical studies investigating the dynamics of Langmuir films on water droplets in the supercooled temperature range would help to improve the understanding of adaptive IN.

Acknowledgment. We are grateful for support by the Swiss National Fund in various projects and by the European Commission through the integrated project SCOUT-O3.

References and Notes

(1) Koop, T. *Z. Phys. Chem.* **2004**, *218*, 1231−1258.

(2) Baker, M. B. *Science* **1997**, *276*, 1072−1078.

(3) Krog, J. O.; Zachariassen, K. E.; Larsen, B.; Smidsrød, O. *Nature* **1979**, *282*, 300−301.

(4) Bowles, D. J.; Lillford, P. J.; Rees, D. A.; Shanks, I. A., Eds. *Phil. Trans. R. Soc. London B* **2002**, *357*, 829−955.

(5) Gavish, M.; Popovitz-Biro, R.; Lahav, M.; Leiserowitz, L. *Science* **1990**, *250*, 973−975.
(6) Popovitz-Biro, R.; Wang, J. L.; Majewski, J.; Shavit, E.; Leiserowitz, L.; Lahav, M. *J. Am. Chem. Soc.* **1994**, *116*, 1179−1191.
(7) Majewski, J.; Popovitz-Biro, R.; Bouwman, W. G.; Kjaer, K.; Als-Nielsen, J.; Lahav, M.; Leiserowitz, L. *Chem. Eur. J.* **1995**, *5*, 304−311.
(8) Seeley, L. H.; Seidler, G. T. *Phys. Rev. Lett.* **2001**, *87*, 055702, DOI: 10.1103/PhysRevLett.87.055702.
(9) Pruppacher, H. R.; Klett, J. D. *Microphysics of clouds and precipitation*; Kluwer: Dordrecht, The Netherlands, 1997.
(10) Atkins, P. W. *Physical Chemistry*, 4th ed.; Oxford University Press: Oxford, UK, 1990.
(11) Smith, R. S.; Kay, B. D. *Nature* **1999**, *398*, 788−791.
(12) Seinfeld, P. W.; Pandis, S. N. *Atmospheric Chemistry and Physics*; John Wiley & Sons, Inc.: New York, 1998.
(13) Lide, D. R. *Handbook of chemistry and physics*, 82nd ed.; CRC Press LLC: Boca Raton, FL, 2001.
(14) Krämer, B.; Hübner, O.; Vortisch, H.; Wöste, L.; Leisner, T.; Schwell, M.; Rühl, E.; Baumgärtel, H. *J. Chem. Phys.* **1999**, *111*, 6521−6527.
(15) Duft, D.; Leisner, T. *Atmos. Chem. Phys.* **2004**, *4*, 1997−2000.
(16) Benz, S.; Megahed, K.; Möhler, O.; Saathoff, H.; Wagner, R.; Schurath, U. *J. Photochem. Photobiol.* **2005**, *176*, 208−217.
(17) Stöckel, P.; Weidinger, I. M.; Baumgärtel, H.; Leisner, T. *J. Phys. Chem. A* **2005**, *109*, 2540−2546.
(18) Kabath, P.; Stöckel, P.; Lindinger, A.; Baumgärtel, H. *J. Mol. Liq.* **2006**, *125*, 204−211.
(19) Hobbs, P. V. *Ice Physics*; Larendon Press: Oxford, UK, 1974.
(20) Murphy, D. M.; Koop, T. *Q. J. R. Meteorol. Soc.* **2005**, *131*, 1539−1565.
(21) Koop, T.; Luo, B. P.; Biermann, U. M.; Crutzen, P. J.; Peter, T. *J. Phys. Chem. A* **1997**, *101*, 1117−1133.
(22) Knopf, D. A.; Koop, T. *J. Geophys. Res.* **2006**, *111*, D12201, DOI: 10.1029/2005JD006894.
(23) Popovitz-Biro, R.; Lahav, M.; Leiserowitz, L. *J. Am. Chem. Soc.* **1991**, *113*, 8943−8944.
(24) Seeley, L. H.; Seidler, G. T. *J. Chem. Phys.* **2001**, *114*, 10464−10470.
(25) To obtain this point, a 3 μL droplet coated with the nonadecanol/mineral oil solution was kept at 266.15 K in the DSC and the time until the droplet was frozen was measured three times. The corresponding mean ice nucleation rate coefficient was calculated with eq 15.
(26) Majewski, J.; Margulis, L.; Jacquemain, D.; Leveiller, F.; Bohm, C.; Arad, T.; Talmon, Y.; Lahav, M.; Leiserowitz, L. *Science* **1993**, *261*, 899−902.
(27) Ochshorn, E.; Cantrell, W. *J. Chem. Phys.* **2006**, *124*, 054714, DOI: 10.1063/1.2166368.
(28) Cantrell, W.; Robinson, C. *Geophys. Res. Lett.* **2006**, *33*, L07802, DOI: 10.1029/2005GL024945.